EPM2021

Riga . LATVIA . June 13-17

Poster session

10th international conference

Electromagnetic Processing of Materials

Riga, Latvia, Tuesday, June 15.

Time 17:00-19:00

UNIVERSITY OF LATVIA

Chairman: Artūrs Brēķis

1.	Institute of Numerical Modelling, University of Latvia	**Kirils Surovovs** A. Kravtsov J. Virbulis	The role of numerical modelling in the diameter increase of silicon crystals grown from pedestal	17:10-17:20
2.	State Key Laboratory of Advanced Special Steel & Shanghai Key Laboratory of Advanced Ferrometallurgy, Shanghai University, Shanghai	**Haibiao Lu** Bin Li Yunbo Zhong et al.	Numerical simulation of EMS position on flow, solidification and inclusion transport in slab continuous casting	17:20-17:30
3.	Institute of Electrotechnology, Leibniz University Hannover, Hannover, Germany	**Mattia Guglielmi** I. Smolyianov J. Vencels E. Baake	Investigation of an electromagnetic stirring process by parallel numerical simulations in ANSYS FLUENT and OPEN FOAM	17:30-17:40
4.	LU Institute of Physics	**Ervins Blumbergs** J. Freibergs E. Platacis et al.	Study of the degree of cadmium reduction from cadmium oxide by the electroslag method under different conditions	17:40-17:50
5.	Institute of Thermodynamics and Fluid Mechanics, Technische Universität Ilmenau, Germany	**Philipp P. Vieweg** Yu. Kolesnikov Ch. Karcher	Experimental study of a liquid metal film flow in a streamwise magnetic field	17:50-18:00
6.	Institute of Thermodynamics and Fluid Mechanics, Technische Universität Ilmenau, Ilmenau, Germany	H. Kalis **Yurii Kolesnikov** Ch. Karcher	Rotating free shear liquid metal flows excited by crossed electric and magnetic fields	18:00-18:10
7.	CENOS EPM Riga	**Mihails Ščepanskis**, V. Geža, D. Berenis, and T. Beinerts	Specialized MHD Software for Rotating Permanent Magnet Stirring on Top of CENOS Platform	18:10-18:20
8.	Univ. Grenoble Alpes, CNRS, Grenoble INP, SIMaP, GRENOBLE, FRANCE	**Amandine Capogna** O. Doche L. Davoust	Effect of a localized MHD body force on the near-wall turbulence	18:20-18:30

Modelling of the pedestal growth of silicon crystals

K. Surovovs[1], A. Kravtsov[2], J. Virbulis[1]

[1] University of Latvia, Jelgavas street 3, LV-1004, Riga, Latvia; email: kirils.surovovs@lu.lv
[2] KEPP EU, Carnikavas street 5, LV-1034, Riga, Latvia

Institute of Numerical Modelling

Introduction

Crucible-free crystal growth methods are used to eliminate melt contamination from crucible walls. One of them is the pedestal method (PM) – an alternative to well-known floating zone (FZ) method. Both these methods are using high-frequency (HF) electromagnetic heating, however in PM method, unlike FZ method, single crystal is being pulled upwards, and the molten zone is located on a pedestal of polycrystalline Si (see Fig. below). PM may be beneficial in comparison to FZ due to simpler process control and lower quality requirements of the polycrystal.

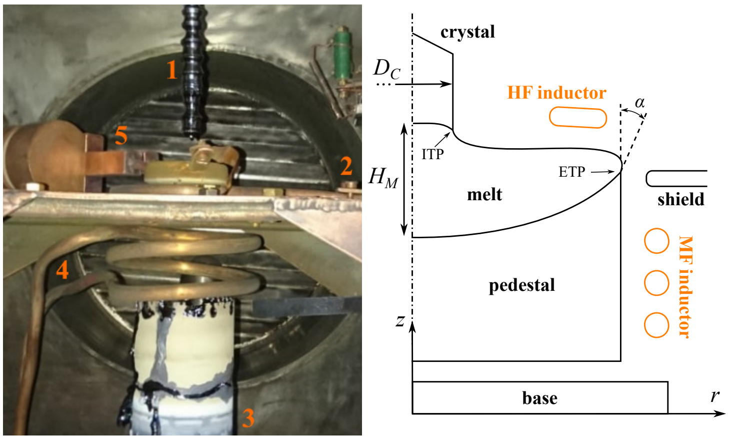

Left – a growth chamber with the crystal seed (1), copper shield (2), pedestal (3), the MF and HF inductors (4, 5). Right – the scheme of the modelled system.

The pedestal method prohibits "needle-eye" inductors: the radius of the grown crystal cannot exceed the inner radius of the inductor [1]. Therefore, the increase of crystal radius leads to the risk of freezing in the centre of molten zone. To decrease this risk, additional pedestal heating is realised using middle-frequency (MF) inductor (see Nr. 4 in the Fig. above).

However, the heating power that can be conducted through the pedestal side is limited (because the pedestal side should not be melted), therefore precise shape of HF inductor is important to transfer the remaining part of necessary heat towards the centre of the molten zone. The used inductor shape was optimized via gradient method [2] to increase melt height H_M for the cylindrical phase of processes with different crystal diameters D_C. **The present work describes the improvements of the previously developed gradient method for HF inductor optimization**.

Mathematical model

Main principles. The silicon shapes are obtained in axially symmetrical approximation, using previously developed software [2], based on the models described in [3]. Only cylindrical (quasi-stationary) part of the process is considered. To calculate induced heat of HF inductor, high-frequency approximation is used due to relatively small skin layer depth ($\delta = 1.4\,\mathrm{mm}$ for the frequency 2.6 MHz). MF induced heat, however, cannot be approximated by surface heat density only, thus vector potential is calculated in all volume domains [4].

HF inductor optimization. HF inductor was assumed to have axially symmetrical shape. To perform inductor optimization, it was parametrized according to the scheme shown in the Figure: r_{ind} and z_{ind} denote radial and vertical coordinates of the centre of inductor cross-section, $2k_{\mathrm{ind}}$ – cross-section length, c_{ind} – curvature radius, and α_{ind} – the angle of inclination.

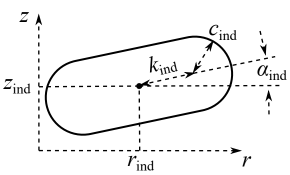

In the previous studies [2, 4], melt height H_M was selected as a target function for the optimization with gradient method. It determines the direction of H_M increase, or ∇H_M, in the phase space of inductor parameters by running 5 additional calculations. Then it modifies the inductor shape in the direction of ∇H_M. If melt height became smaller after the iteration, the step size of modification is reduced twice and inductor shape is returned to the shape from the previous iteration.

Improvement of gradient method. The present poster shows the results of improved gradient method: instead of only H_M, the following formula was used as a traget function:

$$f = \begin{cases} H_M & \text{if} \quad \alpha < 0 \\ H_M \cdot \left(1 - \frac{\alpha}{30}\right) & \text{if} \quad \alpha > 0 \end{cases}$$

where α is the angle between the free surface and vertical at the ETP, see scheme in the Introduction. This formula ensures the decrease of target function if free surface bulges outwards, i.e. when risk of melt spilling occurs.

Simulation results: 100 mm crystal

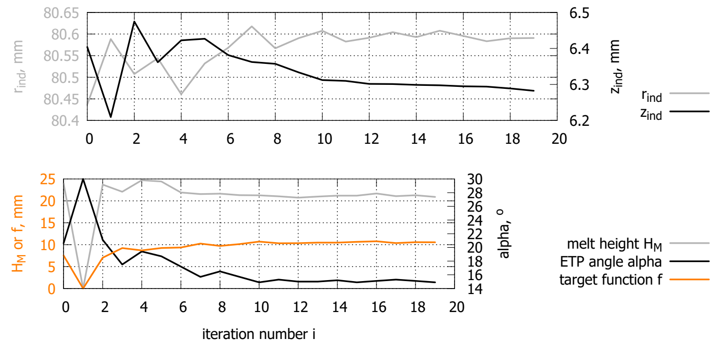

The convergence of inductor and melt parameters during the optimization is shown in Fig. above. Inductor cross-section coordinates r_{ind} and z_{ind} changed only slightly. The improved optimization algorithm prevented α from growing, and the total target function f converged for $\alpha \approx 14^\circ$ and $H_M \approx 27$ mm. However, changes in phase boundaries during the optimization were very small, see Fig. below.

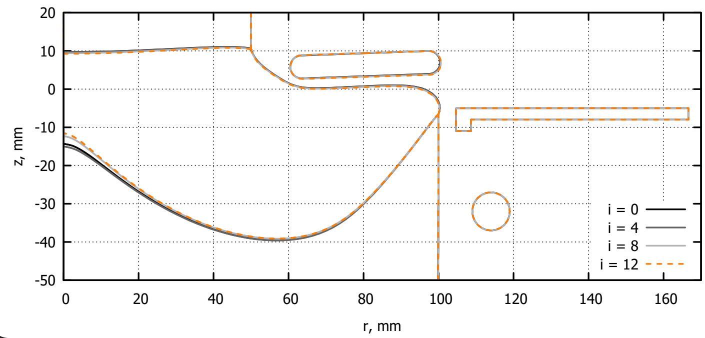

Simulation results: 60 mm and 46 mm crystals

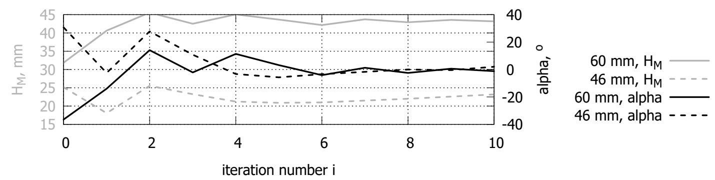

In both cases, α converges to zero, see Fig. above, while changes of H_M are substantial only for the 60 mm crystal. The changes in phase boundaries are more pronounced than in case of 100 mm crystal, see Fig. below.

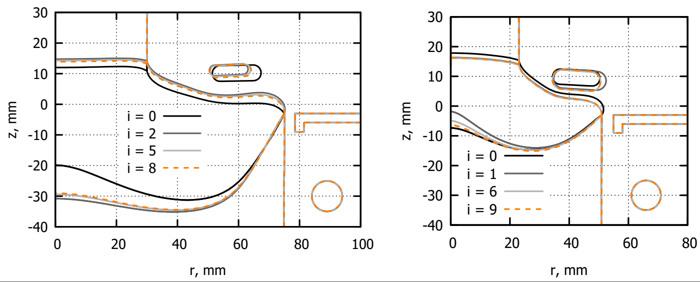

Conclusions

– The HF inductor optimization in the system with 100 mm crystal had been started from the state close to local minimum, therefore changes in parameters during the optimization were very small.
– When $\alpha < 0$, the optimization algorithm maximizes H_M, and α increases due to heat flux redistribution towards melt centre and due to increased zone height. The improved algorithm diminishes α, if $\alpha > 0$. Therefore, the improved algorithm is more useful than the previously proposed one for the prediction of optimal HF inductur shape.

References and acknowledgements

[1] W. Keller, A. Muhlbauer, *Floating-Zone Silicon*, Preparation and Properties of Solid State Materials, vol. 5, (1981).

[2] K. Surovovs, A. Kravtsov, J. Virbulis. *Optimization of the Shape of High-frequency Inductor for the Pedestal Growth of Silicon Crystals*, Magnetohydrodynamics, vol. 55, 353–366 (2019)

[3] G. Ratnieks, A. Muiznieks, A. Muhlbauer. *Modelling of Phase Boundaries for Large Industrial Fz Silicon Crystal Growth With the Needle-eye Technique*, Journal of Crystal Growth, vol. 255, 227–240 (2003)

[4] K. Surovovs, A. Kravtsov, J. Virbulis. *Numerical Modelling for the Diameter Increase of Silicon Crystals Grown with the Pedestal Method*, Journal of Crystal Growth, vol. 563 (2021)

The research leading to these results has been supported by the European Regional Development Fund project "Development of Competence Centre of Mechanical Engineering", contract No.1.2.1.1/18/A/008, Research No. 4.5 "Technological research and silicon production with diameters up to 100 mm for low-current and high-power microelectronic solid state devices".

NACIONĀLAIS ATTĪSTĪBAS PLĀNS 2020
European Union
European Regional Development Fund
IEGULDĪJUMS TAVĀ NĀKOTNĒ

EPM2021
Riga . LATVIA . June 13-17
Proceedings of the 10th international conference

Numerical simulation of EMS position on flow, solidification and inclusion transport in slab continuous casting

Haibiao Lu, Yunbo Zhong, Zhongming Ren, Weili Ren, Zuosheng Lei*

State Key Laboratory of Advanced Special Steel & Shanghai Key Laboratory of Advanced Ferrometallurgy, Shanghai University, Shanghai 200444, China

Introduction

The fluid flow within the mold is of great importance because it effects many complex metallurgical phenomena, including heat transfer, solidification, particle transport and capture, etc. which are closely interrelated and can influence the creation of various defects such as cracks and slivers.

M-EMS has been shown to be one of the most effective countermeasures to improve the molten steel flow. Under this condition, some process parameters, such as the installation position of stirrer, EMS current, etc. should be selected reasonably to reveal the optimal metallurgical effects.

Methods

A three-dimensional mathematical model for slab continuous casting which coupled with electromagnetic field, flow, solidification and inclusion transport has been developed under different EMS positions.

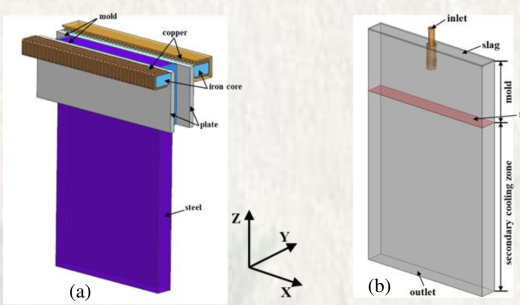

Fig. 1 Schematics of the calculation model:
a) electromagnetic simulation, b) fluid simulation.

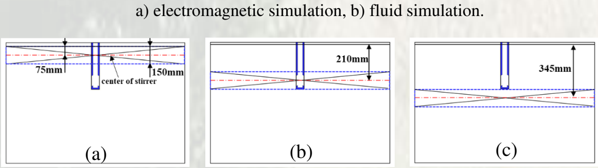

Fig.2 Schematics of stirrer position: a) Case 1, b) Case 2, c) Case 3

Results and discussion

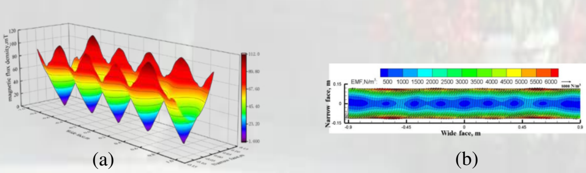

Fig. 3 Distribution of a) magnetic flux density, b) time-average electromagnetic force at stirrer mid-plane with 600A/4.5Hz

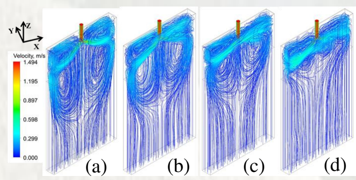

Fig. 4 Comparison of velocity streamline :
a) Case no-EMS, b) Case 1, c) Case 2, d) Case 3

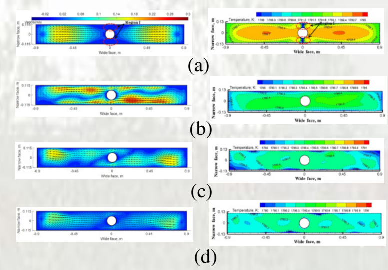

Fig. 5 Distribution of velocity and temperature near free surface: a) Case no-EMS, b) Case 1, c) Case 2, d) Case 3.

When **EMS is not applied**, the flow field within the mold is **classical double-roll** flow pattern, an almost stagnant flow and low temperature are found near the SEN. While **when EMS is applied**, the flow field in the mold changes greatly, the jet flow deviates towards the mold wide face, **the distribution of velocity and temperature change more uniform**, decreasing the stirrer's position, the uniformity decreases.

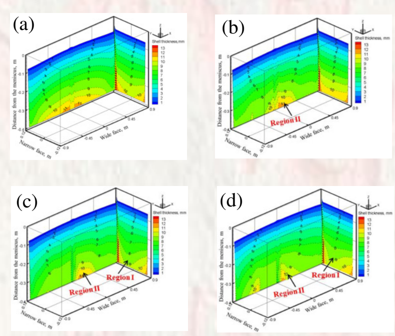

Fig. 6. Spatial variation of solidified shell thickness :
a) Case no-EMS, b) Case 1, c) Case 2, d) Case 3

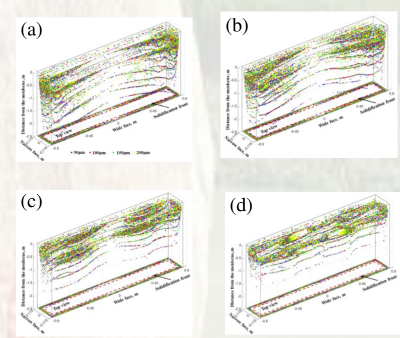

Fig 7. Inclusion distribution entrapped by solidification front :
a) Case no-EMS, b) Case 1, c) Case 2, d) Case 3.

EMS can promote the **uniform growth of solidified shell** especially for that of mold narrow face, but the diagonal flow may result in the remelting of solidified shell at wide face, decreasing the stirrer's position, the remelting phenomenon changes more significant, which may not benefit to the uniformity of solidified shell. Moreover, EMS can **improve the distribution of inclusion at solidification front**.

Conclusion

(1) The flow pattern in the mold changes significantly with the influence of EMS, a diagonal flow pattern which is towards the wide face has generated.

(2) EMS **improve the uniformity of initial solidified shell** and the distribution of inclusion at transverse plane . **Upper stirrer position** is favorable to the uniformity of temperature distribution near the meniscus and **initial solidified shell.**

Acknowledgements

This project financially supported by National Science Foundation of China (NO. U1860107 and 52074181) and the Science and Technology Commission of Shanghai Municipality (No. 19DZ2270200).

EPM2021
Riga . LATVIA . June 13-17

INVESTIGATION OF AN ELECTROMAGNETIC STIRRING PROCESS BY PARALLEL NUMERICAL SIMULATIONS IN ANSYS FLUENT AND OPENFOAM

M. Guglielmi, I. Smolyanov, J. Vencels, E. Baake
Leibniz University Hannover
Ural Federal University
EOF Consulting LLC
guglielmi@etp.uni-hannover.de

Leibniz Universität Hannover

Ural Federal University
named after the first President of Russia B.N.Yeltsin

Aim of the investigation

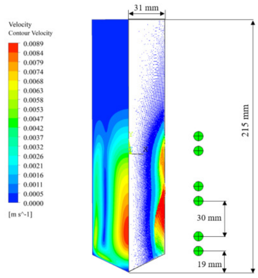

Figure 1: investigation setup. The three-phase inductor can be noticed on the right.

Key problem: numerical simulation of magnetohydrodynamic (MHD) problems can be complex and computationally time consuming; furthermore, accuracy of simulation results must be proved by experimental validations. This work aims to provide the scientific community with new models and knowledge in the frame of numerical simulations of MHD problems: on the first hand, application of unclassical solution methods, like PISO, PIMPLE and Coupled, was compared to the SIMPLE method, which normally accompanies $k-\varepsilon$, $k-\omega$ and LES turbulence models. On the second hand, simulations of a MHD problem aimed to compare the commercial software Ansys Fluent®, coupled with Ansys Mechanical APDL®, with the open-source OpenFOAM, coupled with Elmer by EOF-Library. Since the interest in the open-source software OpenFOAM is nowadys increasing, numerical results achieved with the two software were compared.

Study subject: electromagnetic stirring (EMS) by travelling magnetic field (TMF). Laboratory-scale cylindrical vessel of plexiglass contained GaInSn melt, which was stirred by the surrounding inductor. Supplied current was three-phase, at the frequency of 50 Hz and maximum amplitude of 100 A. Sequence of phases went from the bottom of the setup to its top, generating a TMF with the same direction.

Figure 2: experimental setup

Description of the mathematical model

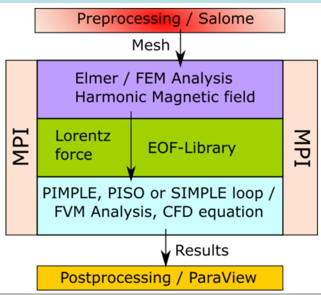

The approach is one-coupling way due to Rm<<1. Governing equations are below:

$$\Delta\mathbf{A} - \mu\sigma\nabla\varphi + \mu\sigma(\mathbf{U}\times\nabla\times\mathbf{A}) = -\mu\mathbf{J}$$

$$\frac{\partial\mathbf{U}}{\partial t} + (\nabla\cdot\mathbf{U})\mathbf{U} - \nu\nabla^2\mathbf{U} = -\nabla\frac{p}{\rho} + \frac{\mathbf{F}}{\rho} + \nabla\nu[2\mathbf{S}]$$

$$\nabla\cdot\mathbf{U} = 0$$

U is the velocity, p is the pressure,

$\mathbf{S}$ is the turbulence term calculating in additional equation according chosen turbulence model,

μ is the magnetic permeability,

φ is the scalar el. potential,

$\mathbf{A}$ is the vector mag. potential,

σ is the electric conductivity,

ν is the kinematic viscosity,

$\mathbf{J}$ is the current density,

$\mathbf{F}$ is the Lorentz force.

Note: the OpenFOAM mesh has only 3D structure. Therefore one-cell wedge mesh, seem as thick part of piece, was created for 2D-axisymetric OpenFOAM task. Elmer mesh has common 2D plane mesh. Because of this, in some cases, there may be no joining between these grids. The 2D mesh will be less than the 3D one. This leads to incorrect values of forces in the problem of hydrodynamics, because when interpolating between these meshes, in the first layer of the hydrodynamic mesh, values from the air will also be taken. To solve this problem, it is necessary to create a mesh for the electromagnetic problem with a near-wall layer 5 and more times less than the first element at the wall in OpenFOAM.

Turbulence model	Subgrid-scale model	Regime	Solution method
$k-\omega$	Standard	Steady-state	SIMPLE, SIMPLEC
		Transient	PISO, PIMPLE, Coupled
	SST	Steady-state	SIMPLE, SIMPLEC
		Transient	PISO, PIMPLE, Coupled
$k-\varepsilon$	Standard	Steady-state	SIMPLE, SIMPLEC
		Transient	PISO, PIMPLE, Coupled
	Realizable	Steady-state	SIMPLE, SIMPLEC
		Transient	PISO, PIMPLE, Coupled
LES	WALE	Transient	SIMPLE, PISO, PIMPLE

Results

Only the average distribution of the Lorentz force was calculated, since its double-frequency component was supposed to influence negligibly the motion of the liquid flow.
Import of the Lorentz force distribution was achieved by a self-written *.txt* file between Ansys Mechanical APDL and Ansys Fluent, and with the EOF-Library between Elmer and OpenFOAM.

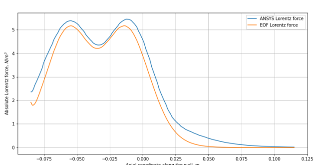

Figure 3: Lorentz force magnitude along the wall. Force measured in Ansys Mechanical APDL is compared with the one in Elmer.

Lorentz force distribution induced within GaInSn melt showed a double peak in the bottom region, consequence of the supplied three-phase current. Forces were directed from the bottom to the top of the system, and maximum amplitude of the force was $F_{max} = 5.6\,\frac{N}{m^3}$. Peak of the force was located at 75 mm from the bottom of the melt domain and almost no force density was generated on the top.

Correct calculation of the Lorentz force distribution was the first fundamental step to guardantee correct fluid dynamic numerical simulation afterwards: very good convergence was achieved between Ansys Mechanical APDL and Elmer in the electromagnetic simulation. Maximum difference between the calculated curves was $\Delta F_{max} = 0.3\,\frac{N}{m^3}$. Qualitative behaviour was almost identical.

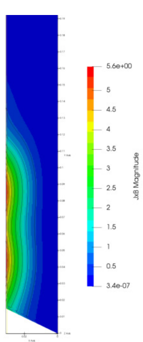

Axial component of velocity was plotted along the axis of the melt, where the highest turbulence was expected to occur: a unique vortex was produced by the application of the TMF, which involved 70% of the GaInSn volume. Velocity went up along the vessel wall, to recirculate downward along the center (Fig.6). Negligible velocity was calculated in the top region of the melt.

Steady-state regime: good similarity was achived between numerical results in Ansys Fluent and OpenFOAM in 80% of the simulated cases. In both software, maximum axial velocity calculated along the axis was $v_{max} = 8.6\,\frac{mm}{s}$, with the peak located at 30 mm from the bottom of the vessel. In Ansys Fluent, $k-\omega$ SST SIMPLE turbulence model had the highest convergence with OpenFOAM. Remarkable difference was noticed only for the $k-\varepsilon$ SIMPLE and $k-\omega$ PISO models calculated in Ansys Fluent: simulated velocity showed a maximum of $v_{max} = 4.89\,\frac{mm}{s}$, located at the height of 75 mm from the bottom. Behaviour of the flow is right now under validation by experimental activities at the Institute of Electrothermal Processing in Hannover.

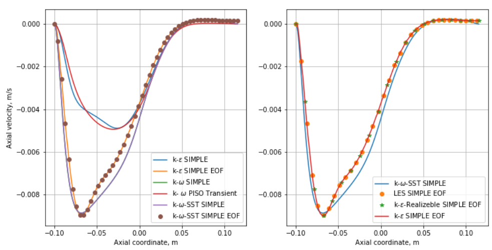

Figure 5a: axial velocity along the axis of the liquid GaInSn, comparison between Ansys Fluent and OpenFOAM numerical results in transient regime.

Transient regime: evolution of the flow along the axis was confirmed, as good convergence between the two software. Turbulence models $k-\varepsilon$ and $k-\omega$ showed that the fluid flow fully developed after 55 seconds and the peak of velocity moved from a higher position of 75 mm to 30 mm from the bottom of the vessel. Maximum velocity of $8.6\,\frac{mm}{s}$ was achieved in transient LES PISO, LES PIMPLE and $k-\varepsilon$ Realizable PISO models carried out in OpenFOAM and in the $k-\omega$ SST SIMPLE model in Ansys. Notable qualitative and quantitative difference was noticed again in the $k-\varepsilon$ SIMPLE and $k-\omega$ PISO models performed in Ansys Fluent, which calculated a maximum velocity along the axis of $4.8\,\frac{mm}{s}$ after 100 seconds of the simulation.

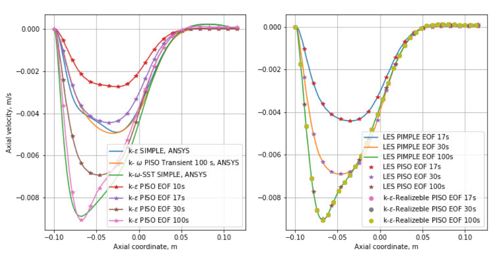

Figure 5b: axial velocity along the axis of the liquid GaInSn, comparison between Ansys Fluent and OpenFOAM numerical results in transient regime.

Figure 6 summarizes the results achieved with Ansys Fluent and OpenFOAM. Case a) shows the velocity contour performed in OpenFOAM with the $k-\varepsilon$ SIMPLE turbulence model: highest recirculation of velocity occurred along the axis of the melt, with a peak on its bottom region, at the height of 30 mm. Picture b) shows the velocity vector field simulated in Ansys Fluent with the $k-\varepsilon$ SIMPLE model. Direction of the generated torodal vortex was evidenced, as the different distribution of velocity compared to the one on OpenFOAM.

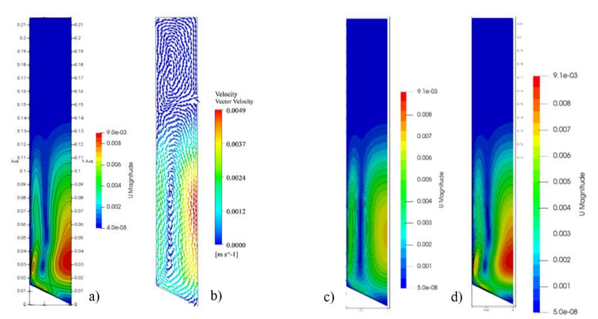

Figure 6: velocity contour and velocity vector field within liquid GaInSn. Comparison between Ansys Fluent and OpenFOAM, both in steady-state ad transient regime.

Pictures c) and d) show the evolution of velocity calculated with LES in OpenFOAM: a stable vortex was calculated, whose peak moved over time towards the bottom of the melt volume. Recirculation of the flow occurred also next to the corner of the melt. Final distribution of the flow field was equal to the one calculated in steady-state regime.
Application of the LES model in Ansys Fluent shows, on the other hand, strong oscillations of the flow peak along the vertical direction, which partially fits with the previously described results.

Conclusions

An electromagnetic stirring process was investigated under the application of travelling magnetic field. Numerical simulations were performed in parallel with the commercial software Ansys Fluent and the open-source software OpenFOAM, and their results were compared, in terms of velocity field within the liquid GaInSn. Unclassical solution methods (PISO, PIMPLE, Coupled) were applied, to improve the accuracy of numerical simulations of MHD problems.
Good convergence between Ansys Fluent and OpenFOAM was achieved in 80% of the simulated cases: steady-state $k-\varepsilon$ Realizable and PISO, $k-\omega$ SST SIMPLE and PISO gave the same qualitative and quantitative results, with maximum velocity of $8.6\,\frac{mm}{s}$ and a peak located at 30 mm from the bottom of the melt. Remarkable difference was noticed for $k-\varepsilon$ SIMPLE model, whose maximum velocity was $4.89\,\frac{mm}{s}$, with a peak shifted towards the top of the melt. Transient simulations in LES, $k-\varepsilon$ and $k-\omega$ confirmed the found steady-state results and calculated that fluid flow develops after 55 seconds. Evident divergence was still remarked between the $k-\omega$ PISO and all the other models performed in OpenFOAM.
Convergence between Ansys Fluent and OpenFOAM was completely satisfying, and the application of unclassical solution methods opened new alternatives in the simulation of MHD problems. This work aims to be extended to a 3D model and to validate the numerical results by experimental activities.

References

[1] F.N. Sarapulov and V.E. Frizen. Electromagnetic model of a multiphase inductive crucible furnace. *Russian Electrical Engineering*, vol. 84 (2013), no. 3, pp. 165-170

[2] D. Valters and N.C. Markatos. Introduction to MHD simulation software, Laboratory for mathematical modelling of environmental and technological processes. *University of Latvia* (2019), pp. 18

[3] J. Vencels, P. Råback and V. Geža. EOF-Library: open-source Elmer FEM and OpenFOAM coupler for electromagnetics and fluid dynamics. *SoftwareX*, vol. 9 (2019), pp. 68-72

[4] K. Moffatt. Electromagnetic stirring. *Physics of Fluids – PHYS FLUIDS 3* (May 1992), pp. 1336-1343

EPM2021 Riga . LATVIA . June 13-17

UNIVERSITY OF LATVIA

STUDY OF THE DEGREE OF CADMIUM REDUCTION FROM CADMIUM OXIDE BY THE ELECTROSLAG METHOD UNDER DIFFERENT CONDITIONS

E. Blumbergs[1]*, J. Freibergs[1], E. Platacis[1], M. Maiorov[1], V. Serga[2]
[1] Institute of Physics University of Latvia, Miera str. 32, Salaspils, LV-2169, Latvia.
[2] Institute of Inorganic Chemistry, Riga Technical University, P. Valdena, 3/7, 1048 Riga, Latvia
**Corresponding author: eblumb@edu.lu.lv*

University of Latvia Institute of Physics

Alkaline nickel cadmium batteries are among the most commonly used industrial power sources. Therefore, the reduction of cadmium (Cd) from waste batteries is an urgent problem for the modern recycling industry. At the same time, cadmium Cd, being a part of the batteries, is highly biotoxic. The reported study describes a new ecologically safe (green) approach to the Cd reduction from cadmium oxide (CdO).

$$2CdO + C \rightarrow t°\mathrm{C} \rightarrow 2Cd + CO_2$$

The report discusses the reaction of cadmium reduction from cadmium oxide in a graphite reactor (see Figure 1, 2), where the temperature is kept below the temperature of cadmium boiling, by electroslag remelting. A ternary chloride composition, containing chlorides of calcium, potassium and sodium, is used as a slag, which allows avoiding the evaporation of cadmium from the reaction volume during reduction from CdO. As a protecting slag layer during reduction which takes place at 6500C, a molar ratio of CaCl2: KCl: NaCl 0.515: 0.0796: 0.405 with the 483 0C melting temperature was chosen. For morphological examination, the obtained products were characterized by electron and optical microscopy, X-ray analysis and by energy dispersive X-ray spectroscopy. The presence of reduced metallic Cd was found (see Figure 3).

During the reduction reaction, it was found that metallic cadmium accumulates with increasing reaction time at the bottom of the crucible under the slag layer.

During the investigation, model experiments were carried out on the reduction of cadmium Cd from cadmium oxide CdO by carbon C under a layer of three-component flux to compare the degree of cadmium reduction and the strength of stirring by a magnetic field induced by a rotating cylindrical radially magnetized permanent magnet placed under the bottom of the crucible, where the reaction of electroslag reduction takes place under the flux layer, and without the influence of the magnetic field induced by the rotating cylindrical radially magnetized permanent magnet, with all other conditions being equal.

Conclusion

During the experiments, reduced cadmium was formed in a finely dispersed form with a particle size of 50 µm to 1 mm. This is because the reduction of cadmium Cd from cadmium oxide CdO with carbon occurs under a layer of a three-component flux, but the flux also prevents the reduced particles of cadmium Cd from joining into a single ingot at the bottom of the crucible. One of the options for solving this problem is the use of a magnetic field created by a rotating cylindrical radially magnetized permanent magnet.

Fig. 1.

Fig. 2.

Fig. 3

ACKNOWLEDGEMENT

The work was supported by project no. Z-LZP2018/16-ZR-N-815.

Experimental Study of a Liquid Metal Film Flow in a Streamwise Magnetic Field

Philipp P. Vieweg[1]*
Y. Kolesnikov[1]
C. Karcher[1]

TECHNISCHE UNIVERSITÄT ILMENAU

Motivation

The increasing digitalization of work and private life, as well as electrification of transport systems requires stable and reliable sources of electricity. Beside the conventional technologies and the recently advanced use of renewable energies, fusion reactors represent another source of electric energy. Liquid metal with a free surface as a working medium is considered there with great interest for the divertor and first-wall protection system. The continuous wetting of a surface with liquid metal is indispensable not only in such applications.

Background

While it is known that the application of strong axial magnetic fields suppresses the instability causing the jet break-up into droplets [1], this present study aims to provide first qualitative data on the suppression of free surface instabilities of liquid metal film flows under the action of strong streamwise magnetic fields for different flow regimes.

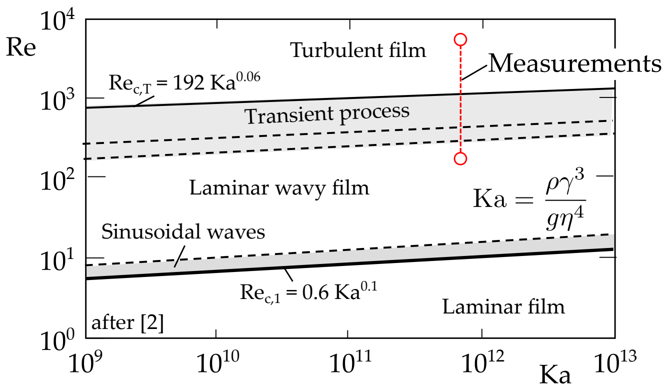

[1] C. Karcher, D. Hernándes, Dynamics of Falling Liquid Metal Droplets and Jets Affected by a Strong Magnetic Field, Magnetohydrodynamics **53**, 739-745 (2017).
[2] F. Al-Sibai, Experimentelle Untersuchung der Strömungscharakteristik und des Wellenübergangs bei welligen Rieselfilmen (PhD thesis, RWTH Aachen, 2004).

Experimental Setup

We designed and built up an experimental setup which allows to study the magnetohydrodynamic influence on the behaviour of liquid metal GaInSn film flows in wavy laminar, transient and turbulent regimes.

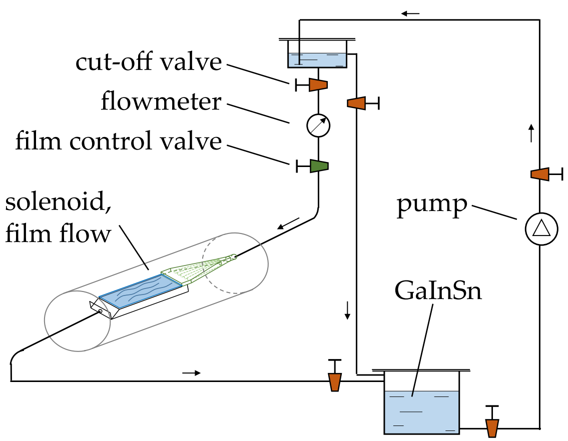

The film flow is inclined while a strong streamwise homogeneous magnetic field covers the full volume of the film with width $w = 23mm$ and length $l = 120mm$.

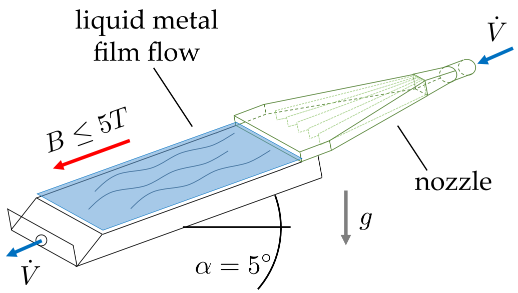

Experimental Results

The film flow's thickness is the characteristic length and develops by

$$t = \sqrt[3]{\frac{3\nu\dot{V}}{w\ g\ sin(\alpha)}} \approx 1mm\,.$$

The dimensionless parameters Reynolds number Re, Hartmann number Ha, and Stuart number N (magnetic interaction parameter)

$$\mathrm{Re} = \frac{\dot{V}}{w\nu} \lesssim 1700 \qquad \mathrm{Ha} = Bt\sqrt{\frac{\sigma}{\eta}} \lesssim 180 \qquad \mathrm{N} = \frac{\mathrm{Ha}^2}{\mathrm{Re}} \lesssim 40$$

with $\eta = \nu\rho$ can be adjusted by controlling the flow rate and the magnetic flux density.

Re = 1400

B [T]	0	0.5	0.75	1.0	2.0
N	0	0.20	0.44	0.79	3.2

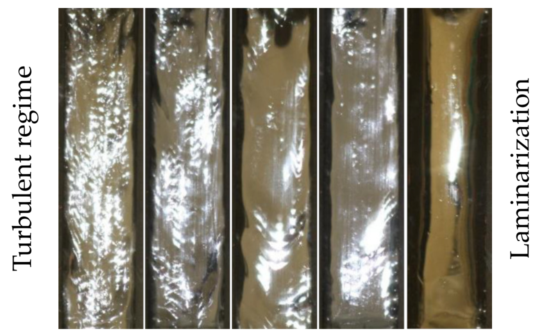

As indicated above, a streamwise magnetic field is capable of suppressing the free surface instabilities originating from all investigated initial flow regimes by dampening the motions perpendicular to the magnetic field. Thus, the flow regime at some Re *with* magnetic field is similar to a flow regime *without* magnetic field but at lower Re.

[1] Institute of Thermodynamics and Fluid Mechanics
University of Technology Ilmenau, Germany

*philipp.vieweg@tu-ilmenau.de

Electromagnetic Processing of Materials
Riga, Latvia, 13-17 June 2021

The authors thankfully acknowledge financial support by the Deutsche Forschungsgemeinschaft (DFG) within the framework of the Research Training Group "Lorentz force velocimetry and Lorentz force eddy current testing" under grant GRK 1567.

Rotating Free Shear Liquid Metal Flows Excited by Crossed Electric and Magnetic Fields

EPM'2021 Topic 1 H. Kalis, Yu. Kolesnikov, Ch. Karcher (LU Riga, Latvija; TU Ilmenau, Germany)

- Such flows in an axial magnetic field have the significant applications for technical hydrodynamics and astrophysics, *Lenert*, 1970 [1].

1. Formulation of the problem

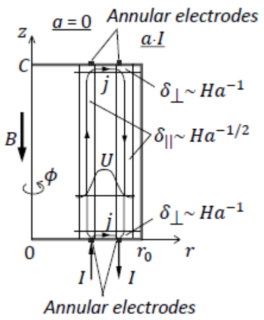

Figure 1: Free shear flows excited by interaction of injected electric current and applied magnetic field (picture at strong magnetic field).

Conductive liquid is in a cylindrical container of radius r_0 and height C placing in an axial uniform magnetic field B:

$$\Omega = \{(r,z,\varphi):\ 0 \le r \le r_0;\ 0 \le z \le C;\ 0 \le \phi \le 2\pi\}$$

By Moffat, 1964 [2]: In a strong magnetic field the inertial forces can be neglected compared with magnetic and viscous forces, so **the flow pattern depends only on the Hartmann number and the specified boundary conditions:**

$$\frac{\partial}{\partial r}\left(\frac{1}{r}\frac{\partial rU}{\partial r}\right)+\frac{\partial^2 U}{\partial z^2}+Ha\frac{\partial H}{\partial z}=0,\qquad r\in(0,1),\qquad z\in(0,C/r_0),$$

$$\frac{\partial}{\partial r}\left(\frac{1}{r}\frac{\partial rH}{\partial r}\right)+\frac{\partial^2 H}{\partial z^2}+Ha\frac{\partial U}{\partial z}=0,\qquad r\in(0,1),\qquad z\in(0,C/r_0)$$

$$U(0,z)=H(0,z)=U(1,z)=H(1,z)=U(r,0)=U(r,c)=0$$
$$H(r,0)=H_0(r), H(r,c)=a\,H_0(r).$$

By means of the Matlab operator and asymptotic formula for Bessel functions we obtained the series for: $U(r,z), H(r,z), Q_U, Q_H, j_r, j_z$.

[1] B. LENERT. A partially ionized plasma centrifuge. *Phys. Scripta*. vol. 2, (1970), pp. 106-107.
[2] H.K. MOFFAT. Electrically driven steady flows in magnetohydrodynamics. *Appl. Mech., Proc.*: The 11th International Congress of Applied Mechanics, Munich, Germany (1964)

2. Results

During calculations, we used fluid with physical properties of liquid metal, like „galinstan".

$a = 0$ *Current is injected in liquid via one pair of electrodes on the bottom*

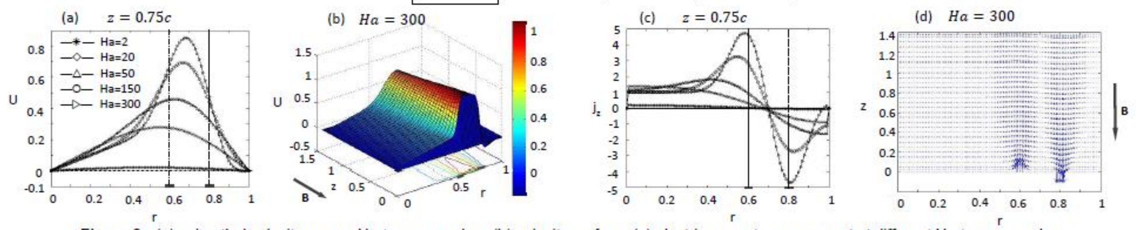

Figure 2: (a) azimuthal velocity versus Hartmann number; (b) velocity surface; (c) electric current z-component at different Hartmann numbers; (d) electric current vectors with $z-$ and $r-$components in the vertical cross-section.

$a = 1$ *Current is injected in liquid via two pairs of electrodes on the end walls*

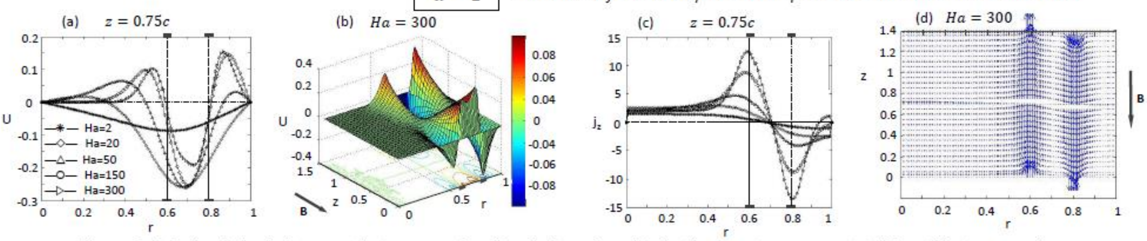

Figure 3: (a) azimuthal velocity versus Hartmann number; (b) velocity surface; (c) electric current z-component at different Hartmann numbers; (d) electric current vectors with $z-$ and $r-$components in the vertical cross-section.

3. Conclusions

- Analytical solutions for the free axisymmetric shear flows in uniform axial magnetic field are received.
- At one- and two-side supplies of electric current ($a = 0$ and $a = 1$) in a strong field, a potential core, two side shear layers, parallel to the field, and two Hartmann layers on the end walls arise.
- The radial electric current in the flow cores is essentially smaller (up to 60-fold) than the axial current in the side layers, but is sufficient to provide the Lorentz force for compensation of friction forces in the cores.
- Existing of large velocity gradients and the inflection points in velocity profiles relates these flows to highly unstable flows.

University of Latvia
Institute of Mathematics and Computer Science
3 Jelgavas street, LV-1002 Riga, Latvia
E-Mail: harijs.kalis@lu.lv
http://www.lu.lv

UNIVERSITY OF LATVIA

Technische Universität Ilmenau
Institut für Thermo- und Fluiddynamik, PO Box 100565, 98684 Ilmenau
Tel.: +49 3677 69 2422 / 2455, Fax: +49 3677 69 2411
E-Mail: yuri.kolesnikov@tu-ilmenau.de, christian.karcher@tu-ilmenau.de
http://www.tu-ilmenau.de/TTD/

TECHNISCHE UNIVERSITÄT ILMENAU

CASE STUDY: Specialized MHD Software for Rotating Permanent Magnet Stirring on Top of CENOS Platform

M. Ščepanskis , V. Geža, D. Berenis, T. Beinerts
CENOS & EPM Riga

CENOS Platform integrates modeling open-source tools and libraries into seamless workflow allowing to configure **industry-specific simulation apps** of exceptional ease-of-use.

Academic users can get free license for non-commercial use, as well as access to app-building API.

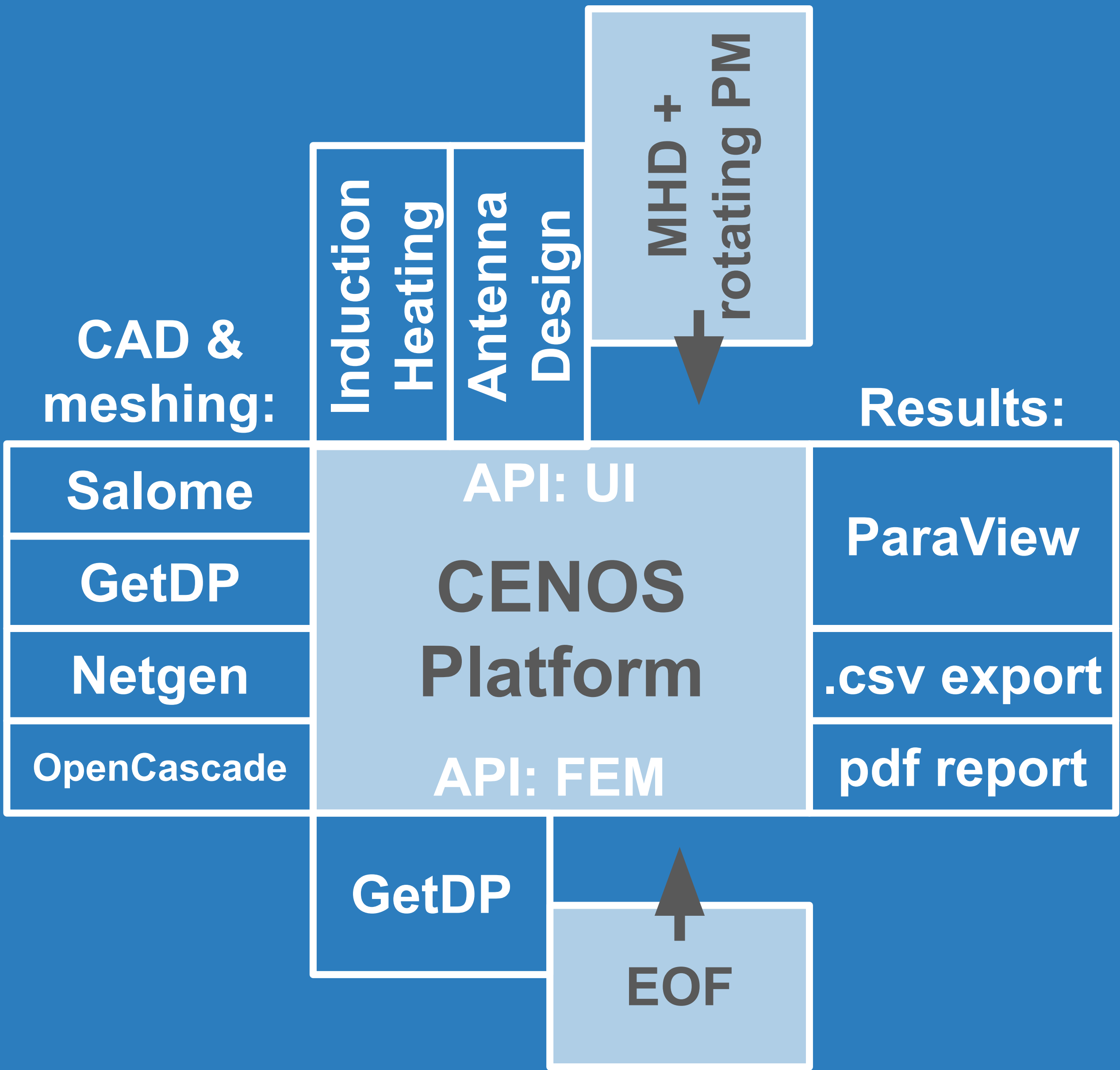

MHD - rotating PM app building is funded by BOWI project (EU public grant) to be launched by October 2021

Effect of localized MHD body force on the near-wall turbulence

A. CAPOGNA, O. DOCHE, S. TARDU, J. SCHILLINGS , L. DAVOUST

Magnetic field distribution

We study a turbulent channel flow ($Re = 4200$) under a uniform magnetic field on a limited zone near the walls. Three thicknesses of boundary layer are studied here : $0.17h$ (viscous and buffer sublayers), $0.3h$ (logarithmic layer), and h (whole channel). Two magnetic orientations are taken into account : streamwise (B_x) and spanwise (B_z).

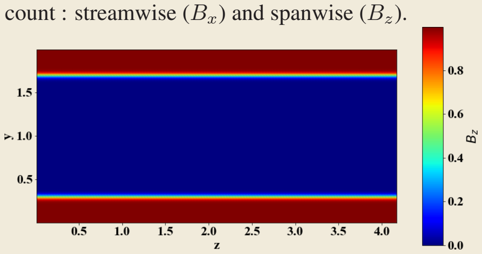

Magnetic distribution in the spanwise case.

Non-dimensionnalization

Two non-dimensionnalized equations in wall units descibe the MHD phenomena:

$$\frac{\partial \boldsymbol{v}}{\partial t} + (\boldsymbol{v}\cdot\boldsymbol{\nabla})\boldsymbol{v} = -\boldsymbol{\nabla}P + \Delta \boldsymbol{v} + N_\tau \boldsymbol{J}\times\boldsymbol{B}$$

$$\boldsymbol{J} = (\boldsymbol{\nabla}\phi + \boldsymbol{v}\times\boldsymbol{B})$$

- $u_\tau = \sqrt{\tau_w/\rho}$ the shear velocity of the unmanipulated channel flow.
- $\tau_w = \nu\partial u/\partial y$ the wall shear stress.
- $\delta_\nu = \nu/u_\tau$ the caracteristic length.
- $Re_\tau = u_\tau h/\nu$ the Karman number.
- $Ha = B_0 h\sqrt{\sigma/(\rho\nu)}$ the Hartmann number.
- $N_\tau = (Ha/Re_\tau)^2$ the Stuart number (or interaction parameter) in wall units.

The Stuart parmeter scaled by the wall units seems to be sufficient to descibe the whole MHD turbulent case.

Conclusion

- A new interaction parameter N_τ can be found in wall turbulence MHD. This parameter is sufficient to descibe a whole near-wall MHD turbulent case.
- In any case, B_x is less relevant since the source and annihilation parts of the MHD transport terms counteract each other.
- For B_z, the annihilation MHD transport terms dominate. Even if there is no full relaminarization when the magnetic field is applied over a $0.3h$-thick boundary layer, some clear relaminarized turbulent flow features are observed.
- The magnetic field needs to reach the logarithmic layer to quasi-relaminarize the turbulent channel flow.

References

[1] D. Lee, H. Choi. Magnetohydrodynamic turbulent flow in a channel at low magnetic Reynolds number In *Journal of Fluid Mechanics 2001*

[2] S. Tardu. Wall Turbulence Control J. Wiley and Sons 2017

Aknowlegdements

All the computations presented in this paper were performed using the Froggy platform of the GRICAD infrastructure (`https://gricad.univ-grenoble-alpes.fr`), which is supported by the Rhône-Alpes region (GRANT CPER07_13 CIRA) and the Equip@Meso project (reference ANR-10-EQPX-29-01) of the programme Investissements d'Avenir supervised by the Agence Nationale pour la Recherche.

Influence of the severtity parameter N_τ

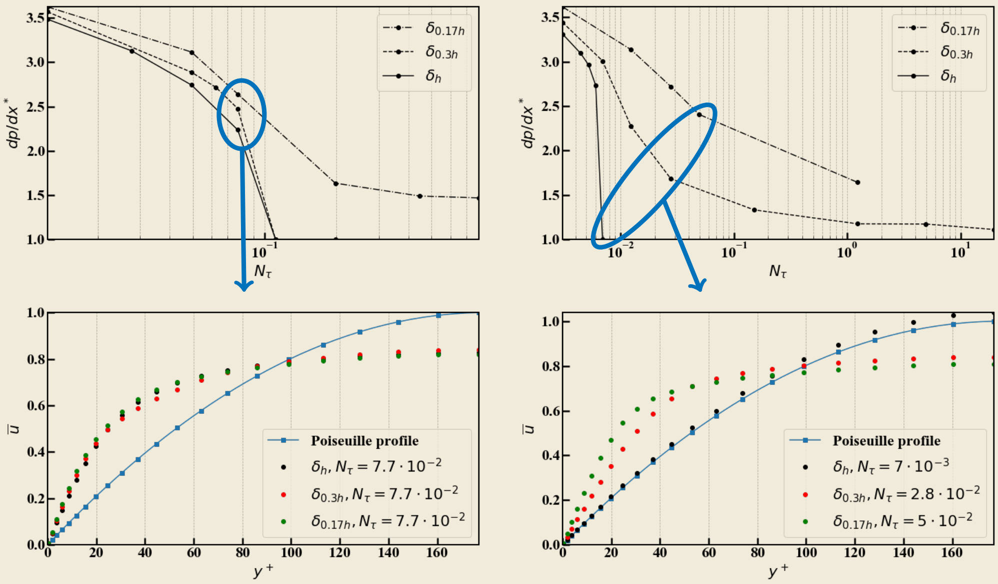

Centerline velocity more affected for the $\delta_{0.3h}$ under B_z case.

Shear stresses transport

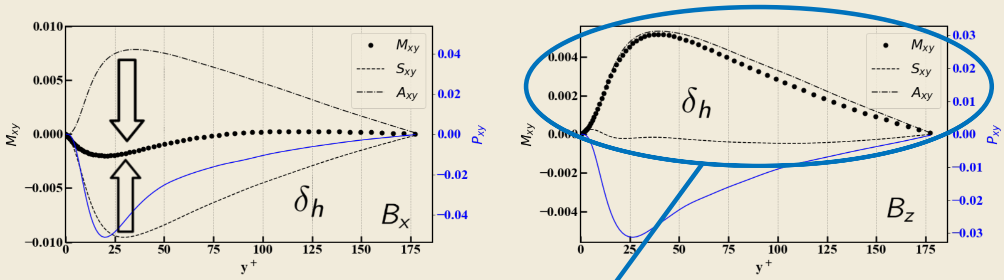

For B_x: the source and annihilation terms for M_{xy} and M_{yy} compensate each other.
$\Longrightarrow$ B_x is not effective.

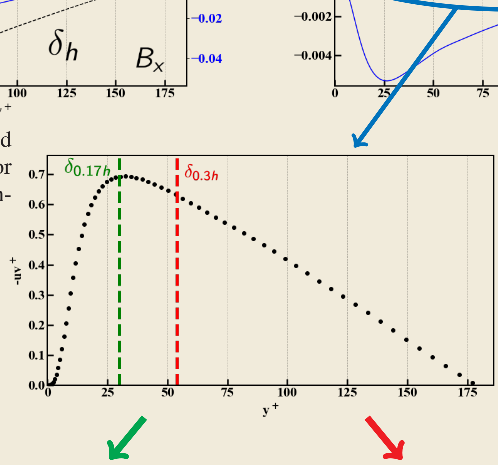

For B_z:
$M_{xy} \approx A_{xy} = -2N_\tau\overline{u_x u_y}$

The efficiency of the magnetic field to relaminarize the flow decreases with the thickness of the magnetically active boundary layer mainly because the annihilation term is limited into a fraction of the wall turbulent field.

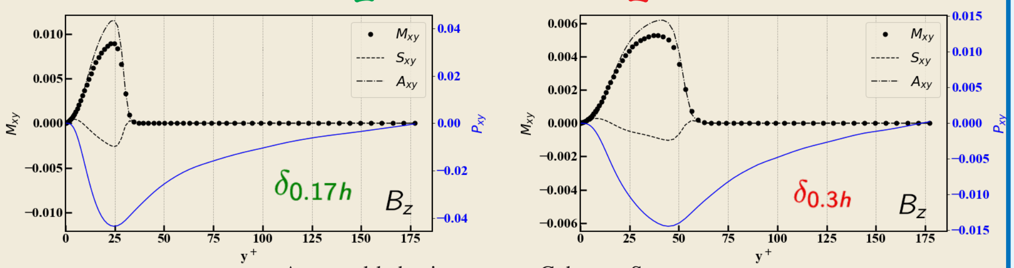

Averaged behaviour over a Coherent Structure:
M_{xy} flattened for the $\delta_{0.17h}$ case.